RSC Advances

PAPER

View Article Online
View Journal | View Issue

Cite this: *RSC Adv.*, 2019, **9**, 41955

A new ratiometric fluorescence assay based on resonance energy transfer between biomass quantum dots and organic dye for the detection of sulfur dioxide derivatives†

Jingjin Zhao, ‡[ab] Yao Peng,‡[a] Keqin Yang,[a] Yunyun Chen,[a] Shulin Zhao *[a] and Yi-Ming Liu *[b]

Received 13th November 2019
Accepted 10th December 2019

DOI: 10.1039/c9ra09437g

rsc.li/rsc-advances

Sulfur dioxide (SO_2) is considered as the fourth gas signal molecule after nitric oxide (NO), carbon monoxide (CO) and hydrogen sulfide (H_2S). It plays important roles in several physiological processes. Therefore, the design and synthesis of nanoprobes for the detection of SO_2 derivatives in cells is of great significance. Herein, we report a new ratiometric fluorescence nanoprobe based on resonance energy transfer (RET) between biomass quantum dots (BQDs) and organic dye (DMI) for the detection of SO_2 derivatives. The proposed ratiometric fluorescence assay allows the determination of HSO_3^- in the range of 1.0 to 225 μM with a detection limit of 0.5 μM. Importantly, the proposed ratiometric fluorescence nanoprobe exhibits a high photostability and good selectivity for HSO_3^- over other chemical species including H_2S and biological mercaptans. Quantitation of HSO_3^- in cell lysates by using the nanoprobe is demonstrated.

1. Introduction

Sulfur dioxide (SO_2) is an irritant gas and a major atmospheric pollutant. It is usually in the form of SO_3^{2-} and HSO_3^- in solution.[1,2] *In vivo*, SO_2 is considered as the fourth gas signal molecule after nitric oxide (NO), carbon monoxide (CO) and hydrogen sulfide (H_2S).[3] SO_2 can be produced in cytoplasm and mitochondria by enzymatic catalysis of sulfur-containing amino acids and oxidation of H_2S.[4] Endogenous SO_2 has unique biological activity and plays an important role in a series of physiological and pathological processes, such as improving antioxidant capacity, regulating vascular structure and function, *etc.*[5,6] On the other hand, studies have shown that abnormal production of endogenous SO_2 derivatives is associated with certain diseases such as neurological disorders[7] and lung cancer.[8] Therefore, the development of analytical methods with good repeatability and sensitivity for the detection of SO_2 derivatives in cells is of great significance.

Current methods for the detection of HSO_3^- (a major form of SO_2 existing in living systems) include electrochemical detection method,[9] high performance liquid chromatography (HPLC),[10] capillary electrophoresis,[11] *etc.* These methods have limitations such as poor reproducibility, un-satisfactory assay sensitivity, or cumbersome operation. In recent years, fluorescence based methods have received attention due to their high sensitivity, good selectivity, and short analysis time. Several fluorescent probes for HSO_3^- detection were developed based on nucleophilic reactions with aldehydes, levulinic acid cracking and coordination interactions.[12–18] However, these fluorescent probes are susceptible to interference from endogenous compounds such as biological mercaptans, proteases and esterases. In addition, it's well known that fluorescence assays based on changes in single-wavelength fluorescence intensity (increase or decrease) are affected by probe concentration, instrument stability, and background interference of the test system.[19–21]

Ratiometric fluorescence assay is more accurate than single-wavelength fluorescence intensity detection because it eliminates most of the interference caused by light bleaching, instrument instability, and sample matrix background by self-calibration on two emission bands. In recent years, many ratio fluorescence probes were developed for SO_2 assay.[22–31] However, most of these probes were designed based on the mechanism of intramolecular charge transfer (ICT). Such probes have shortcomings such as low fluorescence resolution, and being susceptible to the influence from other biological mercaptan. On the other hand, these organic small molecular fluorescent probes are prone to photobleaching when exposed to light, so their optical stability is not very good. Therefore, it is highly significant to develop stable,

[a]*State Key Laboratory for the Chemistry and Molecular Engineering of Medicinal Resources, Guangxi Normal University, Guilin, 541004, China. E-mail: zhaoshulin001@163.com*

[b]*Department of Chemistry and Biochemistry, Jackson State University, 1400 Lynch St., Jackson, MS 39217, USA. E-mail: yiming.liu@msjsu.edu*

† Electronic supplementary information (ESI) available. See DOI: 10.1039/c9ra09437g

‡ These two authors contributed equally to this work.

sensitive and specific ratiometric fluorescence assay for SO_2 derivatives.

Biomass quantum dots (BQDs) are fluorescent carbon based nanomaterials prepared from biomass. They are easy to be prepared, easy to be functionalized, with good photostability, low cytotoxicity and good biocompatibility. Moreover, BQDs with different optical properties can be prepared from different biomass.[32–34] In this work, we prepared a BQDs with green fluorescence emission from corn, and developed a ratiometric fluorescence assay based on resonance energy transfer (RET) between BQDs and organic dye for the detection of sulfur dioxide derivatives (HSO_3^-). The principle of the assay is outlined in Scheme 1. BQDs were prepared from corn by one-step hydrothermal method, and (*E*)-2-(4-(dimethylamino) styrene)-1,3,3-trimethyl-3*H*-indole-1-iodide (DMI) was synthesized by two-step nucleophilic reaction. Both BQDs and DMI obtained showed the fluorescence with maximum emission wavelengths at 518 nm and 595 nm, respectively. DMI had maximum absorption at 549 nm, which was overlapped with the emission spectrum of BQDs. When the two co-exist, fluorescence resonance energy transfer (FRET) occur, which results in the fluorescence intensity of BQDs at 518 nm decreases while that of DMI at 595 nm increases. In the presence of HSO_3^-, absorption of DMI at 549 nm is reduced because HSO_3^- reacts with DMI breaking up the conjugation of the double bonds in DMI, thus diminishing FRET efficiency. As a result, fluorescence emission by DMI is decreased at 595 nm, while fluorescence of BQDs is enhanced at 518 nm. Fluorescence intensity ratio of the system at 518 nm and 595 nm (F_{518}/F_{595}) is linearly proportional to the concentration of HSO_3^- within a certain range. Based on this working principle, a new ratiometric fluorescence method for HSO_3^- detection can be established.

2. Experimental section

2.1 Materials and reagents

Corn was bought from a local vegetable market (Guilin, China). 2,3,3-trimethyl-3*H*-indole, 4-diaminobenzaldehyde, acetonitrile, anhydrous ethanol, iodine methane, $NaNO_2$, KBr, NaCl, KI, Na_2HPO_4, $NaNO_3$, $NaHCO_3$, Na_2CO_3, Na_2S, CH_3COONa, cystine (Cys), glutathione (GSH), H_2O_2, ascorbic acid (AA) and $NaHSO_3$ were purchased from Aladdin reagent company (Shanghai, China). Dulbecco's Modified Eagle Medium (DMEM) was purchased from Thermo Fisher instrument Co., Ltd. (Suzhou, China). Trypsin digestive fluid, fetal bovine serum (FBS), dimethyl sulfoxide (DMSO) and penicillin–streptomycin were purchased from Sigma-Aldrich Company (Saint Louis, MO, USA). The cell lines used in the study: HepG2, MCF-7 and 7702 were purchased from the Cell Bank of the typical Culture Storage Committee of the Chinese Academy of Sciences/Cell Resource Center of the Shanghai Institute of Life Sciences of the Chinese Academy of Sciences (Shanghai, China). Dialysis bag (MWCO = 1 kD, pore size: *ca.*1.0 nm) purchased from Shengong Bioengineering Co., Ltd. (Shanghai, China). All the other chemical reagents in the experiment were analysis pure, and the water used in the experiment was 18.2 MΩ cm ultrapure water.

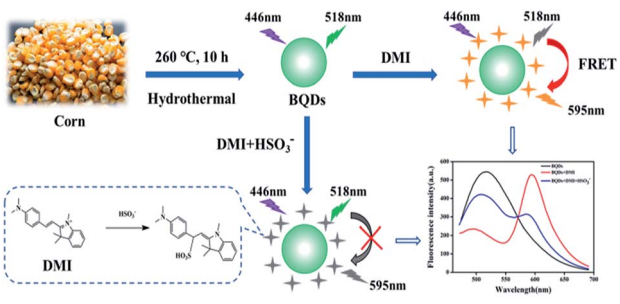

Scheme 1 Schematic illustration of the proposed ratiometric fluorescence assay based on FRET between BQDs and organic dye (DMI) for the detection of SO_2 derivatives.

2.2 Apparatus

The Cary Eclipse fluorescence spectrometer (Agilent Technologies, Santa Clara, CA, USA) was used for recording the fluorescence spectrum. The Cary-60 UV-vis spectrophotometer (Agilent Technologies) was used for recording the UV-vis absorption spectrum. The PerkinElmer Fourier transform infrared (FTIR) spectrometer (PerkinElmer Inc./Thermo Fisher Scientific, Waltham, MA, USA) was used for characterization of the BQDs surface groups. The Rigaku X-ray powder diffractometer (Rigaku Corp., Tokyo, Japan) was used for X-ray diffraction (XRD) analysis. The Philips transmission electron microscope (Philips, Eindhoven, Netherlands) was used to characterize the particle size range of the BQDs. The ESCALAB™ X-ray photoelectron spectrometer (Thermo Fisher, Waltham, MA, USA) was used for elemental analysis of BQDs (XPS). Polytetrafluoroethylene reactor (50 mL, Jinan Henghua technology Co., Ltd.) was used for the synthesis of BQDs. FS-150N ultrasonic processor (Shanghai Biogen ultrasonic instrument Co., Ltd.) was used to prepare cell lysates.

2.3 Synthesis of BQDs

Corn was washed with tap water and ultrapure water, and blow dry the surface. Then, 50 g corn was placed into a mortar, fully grind it and transfer it to the high-pressure reactor lined with polytetrafluoroethylene (volume: 50 mL), 20 mL ultrapure water was added into the high-pressure reactor. Place the high-pressure reactor in the SZCL-3B digital display intelligent temperature control magnetic stirrer for stirring and heating to 260 °C for 10 h for reaction, turn off the heating and continue stirring, and let it cool naturally to room temperature. The mixture in the reactor was filtered with 0.22 μm drainage membrane, and the filtrate was transferred to dialysis bag (MWCO = 1 kD, pore size: *ca.* 1.0 nm). After dialysis in ultrapure water for 12 h, green fluorescent BQDs were obtained.

2.4 Synthesis of DMI

Typically, 3.2 g (20 mmol) 2,3,3-trimethyl-3*H*-indole and 5.68 g (40 mmol) iodine–methane were mixed and dissolved in 10 mL acetonitrile solution. The mixture solution was heated to 60 °C under the protection of argon, and stirred for 11 h under the

reflux of cooling water. The heating was stopped, and after natural cooling to room temperature, the light pink precipitation was obtained. After filtration with qualitative filter paper, the precipitation was washed with ethyl acetate three times. The precipitation was then dried in a vacuum drying oven to obtain a light pink powder (5.8 g).

The light pink powder 0.150 g (0.50 mmol) and 0.12 g (0.75 mmol) 4-(dimethylamine) benzaldehyde were mixed and dissolved in 10 mL ethanol, and placed in a three-necked flask, heated to 180 °C with argon protection, and the cooling water was reflated for 4.5 h to obtain the red solution. The solvent was removed from the rotary evaporator, and a purified organic small molecule compound was obtained by column chromatography (CH_2C_{12}/C_2H_5OH): (*E*)-2-(4-(dimethylamino) styryl)-1,3,3-trimethyl-3*H*-indol-1-ium iodide (DMI, 0.194 g). ^{1}H NMR (400 MHz, $CDCl_3$) δ 8.14 (d, $J = 15.2$ Hz, 2H), 7.49–7.43 (m, 3H), 7.34–7.30 (m, 1H), 6.82 (d, $J = 8.8$ Hz, 2H), 5.32 (s, 1H), 4.17 (s, 3H), 3.20 (s, 6H), 1.99 (s, 1H), 1.80 (s, 6H); ^{13}C NMR (100 MHz, $CDCl_3$) δ 179.0, 155.1, 154.8, 141.8, 141.6, 129.0, 127.6, 122.3, 122.2, 112.7, 112.5, 104.6, 53.4, 50.8, 40.4, 35.1, 27.5. The synthetic rout is shown in the following figure:

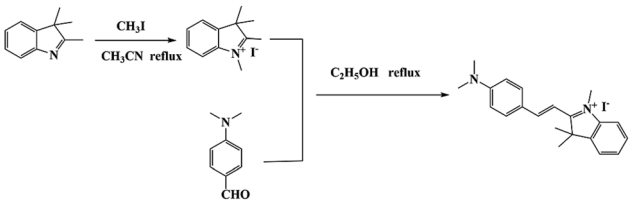

2.5 Preparation of cells lysates

Cells used in the study were HepG2, MCF-7 and 7702 cells. The cell lines were cultured in a DMEM culture medium containing 10% fetal bovine serum, 10 U mL^{-1} penicillin, 10 g mL^{-1} streptomycin, and incubated at 37 °C for 24 h in a 5% CO_2 atmosphere. After digesting with trypsin, the culture medium was removed by centrifugation, and the cells were dispersed in the PBS buffer. This procedure was repeated three times. Then, the cells were resuspended in 1× PBS buffer. A 3 mL volume of above cell suspension was added into the centrifuge tube, and centrifuging for 5 min at a speed of 1000 rpm. Then, the PBS solution was abandoned, 200 μL 1× PBS buffer solutions were used to suspend the cells with a cell density of about 1.43×10^6 cells per mL, and transfer into a 1.5 mL centrifuge tube. The centrifugal tube was put in ice water bath on the ultrasonic instrument, with 80 W ultrasonic power ultrasonic broken for 20 min. After ultrasonic fragmentation, ultrafiltration membranes with a molecular weight cutoff of 10 kDa were used to remove large molecular weight proteins and extract the filtrate was retained for analysis.

2.6 Determination of HSO_3^- in cells lysate

Typically, 20 μL cell lysate was added into 150 μL BQDs-DMI mixture solution (1× PBS : C_2H_5OH = 7 : 3, concentration of DMI is 80 μM), and added a certain amount of ultrapure water to a final volume of 200 μL. After mixing well, the solution was placed for 10 min at room temperature. Then, the fluorescence spectrum of the solution was measured on a fluorescence spectrometer with 446 nm excitation.

3. Results and discussion

3.1 Characterization of BCDs

The morphology, surface functional groups, structure and composition of the BQDs were investigated by transmission electron microscope (TEM), X-ray diffraction (XRD), Fourier transform infrared spectroscopy (FTIR) and X-ray photo-electric spectrometry (XPS), respectively. TEM of BQDs is shown in Fig. 1a. It can be seen from the figure that the prepared BQDs are spherical particles and evenly dispersed, indicating they are water-soluble. The particle size distribution is within the scope of 2.0 to 5.5 nm, average particle size is 3.5 nm (Fig. 1b), and high resolution TEM (HRTEM) (inset in Fig. 1a) shown a clear lattice stripes, lattice constant is 0.315 nm. This corresponds to graphite material (002), indicating that the BQDs consist of graphite-like structures. The crystal surface constant of BQDs is characterized by XRD, and the results are shown in Fig. S1 (ESI).† It can be seen from the figure that the BQDs show a wide diffraction peak at the position of $2\theta = 23.43°$. This diffraction peak corresponds to the amorphous carbon structure crystal plane (002).[35] Functional groups of BQDs surface are characterized by FTIR, and the results are shown in Fig. S2 (ESI).† The peak at 1027 cm^{-1} corresponds to the stretching vibration peak of C–O bond, the peak at 1652 cm^{-1} corresponds to the stretching vibration peak of C=O, the peak at 2939 cm^{-1} belongs to the C–H bond, and the peak at 3367 cm^{-1} corresponds to the stretching vibration peak of O–H/N–H. The results show that on the surface of BQDs hydrophilic groups such as –COOH and –OH are present which lands BQDs with a good water solubility. The element composition and surface bonding of BQDs were characterized by XPS. The results indicated that the BQDs were composed of five elements C, N, O, S and P. The composition was: C 64.44%, N 11.80%, O 23.15%, S

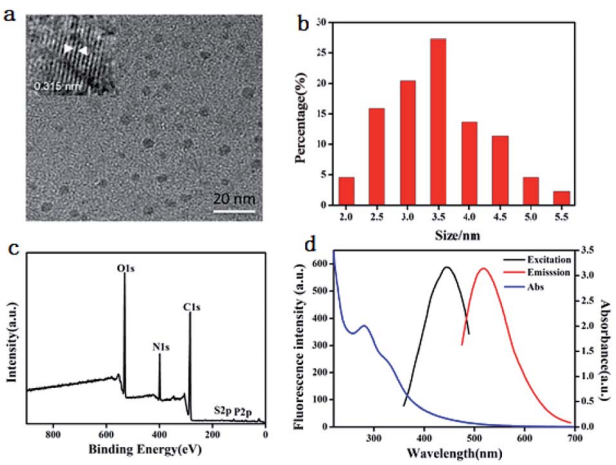

Fig. 1 Characterization of BQDs prepared: (a) TEM and HRTEM images; (b) particle size distribution; (c) XPS spectrum; (d) UV-vis absorption and fluorescence spectra.

0.268% and P 0.332%. According to the overall distribution diagram of element analysis (Fig. 1c), the C 1s characteristic peak appeared at the position of 284.9 eV, the N 1s characteristic peak appeared at the position of 399.7 eV, the O 1s characteristic peak appeared at the position of 531.5 eV, and the S 2p and P 2p characteristic peaks appeared at the position of 163.5 eV and 134.2 eV respectively. As can be seen from the high-resolution spectrum of C 1s (Fig. S3a, ESI†), the signal peak appears at 287.8 eV, 286.3 eV, 285.7 eV, 285 eV and 284.3 eV of C 1s, in which 287.8 eV is C=O bond. 286.3 eV is carbon sp^3 hybrid C–O bond; 285.7 eV is carbon sp^3 hybrid C–N bond; 285 eV is carbon sp^2 hybrid C=C bond; 284.3 eV is carbon sp^3 hybrid C–C/C–H bond.[36] High resolution spectrum of N 1s (Fig. S3b, ESI†) shows that the signal peaks at 400.03 eV and 399.38 eV are respectively the signal peaks of pyrrole N and pyrimidine N.[37] It can be seen from the high-resolution spectrum of O 1s (Fig. S3c, ESI†) that the main bonding of O is O–H (533.3 eV), O–N (532.3 eV), C=O (531.5 eV) and C–O (530.8 eV).[38] Above results show that the surface of BQDs is rich in hydrophilic groups and has good water solubility, which is consistent with the infrared spectrum results.

3.2 Optical performance of the BQDs

To explore the optical properties of BQDs, UV-vis absorption and fluorescence spectra of BQDs were studied. The blue curve in Fig. 1d is the UV-vis absorption spectrum of BQDs, which has the maximum absorption peak at 280 nm. The black curve in Fig. 1d is the fluorescence excitation spectrum of BQDs, with the maximum excitation wavelength of 446 nm. Under the excitation of this wavelength light, the maximum emission peak of BQDs appears at 518 nm (red curve). In addition, the fluorescence emission of BQDs at different excitation wavelengths was investigated. The results are shown in Fig. S4 (ESI).† The fluorescence emission maximum of BQDs was red shifted with the increase of excitation wavelength, indicating that the fluorescence emission spectrum of the BQDs was excitation dependent. At the maximum excitation wavelength of 446 nm, the maximum emission wavelength was 518 nm.

Using quinine sulfate as the reference, the QY of prepared BQDs was obtained to be 14.9%, which is much higher than that of many reported BQDs that were prepared using coffe grounds (3.8%),[39] watermelon peel (6.7%)[40] and sweet potatoes (2.8%)[41] as precursor.

3.3 Stability of BQDs solution

In order to evaluate the stability of BQDs solution, the effects of UV lamp exposure time and solution ion strength on the stability of BQDs were investigated. The fluorescence intensity of BQDs solution was basically unchanged (Fig. S5, ESI†) after exposure to UV lamp (365 nm) for 2 h, indicating that the BQDs solution had good light resistance and bleaching resistance. Fig. S6 (ESI†) shows the effect of ionic strength of the solution on the fluorescence intensity of BQDs. It was found that the fluorescence intensity of BQDs solution was basically unchanged in 0–2.5 M sodium chloride solution. The above results indicate that the BQDs have good anti-bleaching and

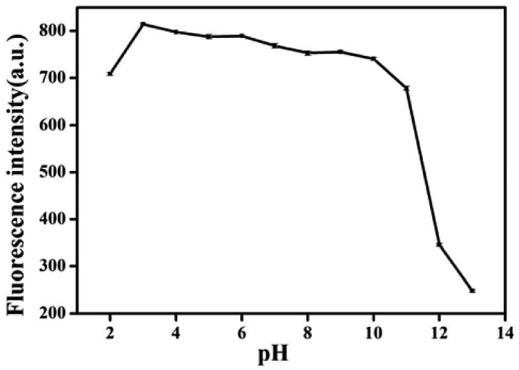

Fig. 2 Effects of pH value on the fluorescence intensity of a BQDs solution.

anti-salt properties, and can be used as fluorescent probes to detect bioactive molecules *in vivo* and *in vitro*. The effect of solution pH value on the fluorescence intensity of BQDs was also investigated. As shown in Fig. 2, when the pH value is within the range of 2.0–3.0, the fluorescence intensity of BQDs solution increases with the increase of the pH value. When pH value is within the range of 10.0–13.0, fluorescence intensity decreases gradually with the increase of pH value of solution. When pH is within the range of 3.0–10.0, fluorescence intensity basically remains unchanged with the increase of pH value of the solution.

3.4 Characterization of DMI

DMI was synthesized by a two-step nucleophilic reaction. The structure of DMI was characterized by mass spectrometry (MS), and the result is shown in Fig. S7 (ESI).† It can be seen from the figure that 305.07 *m*/*z* is the cationic MS peak from DMI, and the abundance of 305.7 *m*/*z* ion is very high, indicating that the purity of the synthesized DMI is very high. In addition, the

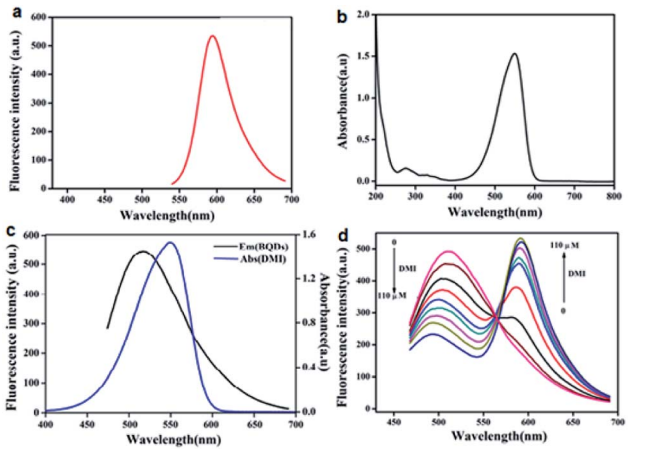

Fig. 3 (a) The fluorescence emission spectrum of BQDs; (b) the UV-visible absorption spectrum of BQDs; (c) the overlap of fluorescence emission spectrum of BQDs and the absorption spectrum of DMI; and (d) fluorescence spectra of BQDs in the presence of DMI at different concentrations.

compound was further identified by ^{1}H NMR and ^{13}C NMR, and the results are shown in Fig. S8 and S9 (ESI),† confirming DMI identity. The fluorescence spectrum and UV-visible absorption spectrum of DMI were studied. As shown in Fig. 3a, the maximum emission wavelength of DMI is at 595 nm. Fig. 3b shows the UV-visible absorption spectrum of DMI. It can be seen from the figure that DMI has the maximum absorption peak near 549 nm.

3.5 FRET between BQDs and DMI

FRET between BQDs and DMI was investigated. The results show that the fluorescence emission spectrum of BQDs and the absorption spectrum of DMI overlap effectively (Fig. 3c), which suggests that when the two coexist FRET will occur. Moreover, with the increase of DMI concentration, the fluorescence intensity of BQDs gradually decreased, while that of DMI gradually increased (Fig. 3d). When HSO_3^- is present in the system, it reacts with DMI, which breaks up the conjugate double bond in DMI (Fig. S10, ESI†), reducing the absorption intensity of DMI (Fig. S11, ESI†) and thus resulting in a decrease in FRET efficiency and recovery of fluorescence emission of BQDs (Fig. S12, ESI†). The results demonstrate that this FRET system is capable of monitoring and quantifying in endogenous HSO_3^- through a ratiometric fluorescence response.

3.6 Ratiometric fluorescence detection of HSO_3^-

To evaluate the FRET system for ratiometric fluorescence assay of HSO_3^-, the response time of HSO_3^- to the system and the linear range of the response were investigated. The results are shown in Fig. S13 (ESI†) and 4. As can be seen from the figure, after adding HSO_3^- the ratio fluorescence intensity (F_{518}/F_{595}) of the system increases gradually with the extension of reaction time, and reaches a maximum after 10 min. With the increase of HSO_3^- concentration, fluorescence intensity of BQDs at 518 nm increases and fluorescence intensity of DMI at 595 nm decreases gradually. F_{595}/F_{518} value and HSO_3^- concentration in the range of 1.0–225 μM show a good linear relationship with a linear regression equation: $F_{518}/F_{595} = 0.00919C + 0.4379$ (where C is concentration of HSO_3^- in μM), $R^2 = 0.9919$. The detection limit was estimated to be 0.5 μM (S/N = 3).

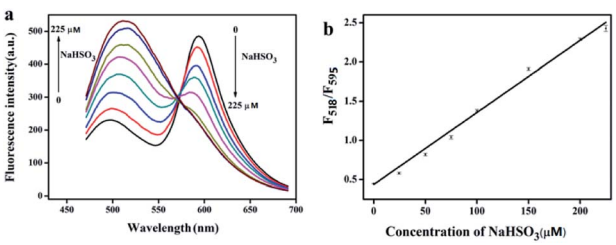

Fig. 4 Ratiometric fluorescence assay of HSO_3^-: fluorescence spectra of BQDs-DIM FRET system in the presence of HSO_3^- at different concentrations (a), and a calibration curve for HSO_3^- quantification (b).

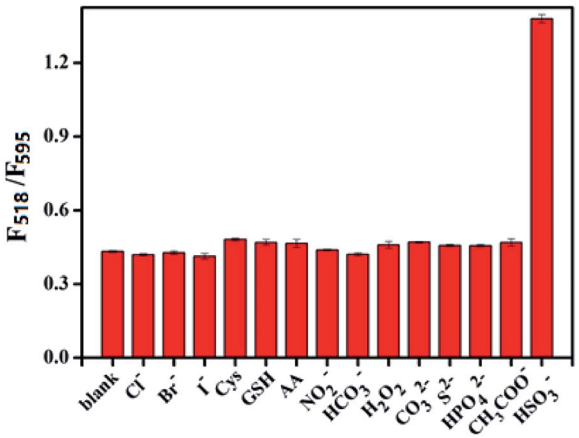

Fig. 5 Specificity of the proposed ratiometric fluorescence assay based on FRET for HSO_3^- detection. Concentration = 100 μM for all species tested.

3.7 Selectivity investigation

In order to assess the selectivity of the proposed assay, the effects of various anions, reactive oxygen species, reducing substances and biological mercaptan on the detection of HSO_3^- were investigated. The results are shown in Fig. 5. When Cl^-, Br^-, I^-, NO_2^-, NO_3^-, HPO_4^{2-}, CH_3COO^-, CO_3^{2-}, HCO_3^-, H_2O_2, GSH, Cys, S^{2-} and ascorbic acid (AA) were introduced into the system, the ratio fluorescence intensity of the system did not change significantly as compared with blank signal. When HSO_3^- was added to the system at the same concentration, the ratio fluorescence intensity of the system increased significantly. These results indicate that the assay has a very good selectivity for HSO_3^-.

3.8 The detection of HSO_3^- in cells lysates

To demonstrate the feasibility of the proposed method for the detection of HSO_3^- in real biological samples, we performed HSO_3^- assay with lysates of HepG2, 7702 and MCF-7 cells. Each sample was measured five times in parallel. HSO_3^- concentration in HepG2, 7702 and McF-7 cell lysates (1.43×10^6 cells per mL) was found 36.8, 34.2 and 30.8 μM, respectively. RSDs of the five parallel assays for HepG2, 7702 and McF-7 cell lysates were

Table 1 Analytical results of HSO_3^- in cells lysates (diluted 10 times)

Sample (cell)	Found (μM)	Added (μM)	Found total (μM)	Recovery (%)
HepG2	3.68	5.0	8.65	99.4
		10.0	13.37	96.9
		20.0	23.59	99.6
7702	3.42	5.0	8.51	101.8
		10.0	13.02	96.0
		20.0	23.24	99.1
MCF-7	3.08	5.0	8.27	103.8
		10.0	13.42	103.4
		20.0	23.22	95.7

0.3%, 0.6% and 0.9%, respectively. The spike and recovery tests were carried out in cell lysates. The recovery was between 95–104% (Table 1), indicating that this method was well suited for the determination of HSO_3^- in cell lysates.

4. Conclusions

A ratiometric fluorescence assay based on RET between BQDs and organic dye (DMI) was developed for the detection of sulfur dioxide derivatives. The proposed method was applied to the quantification of HSO_3^- in HepG2, 7702 and McF-7 cell lysates. The assay has several significant advantages. First, this assay is based on the principle of FRET with BQDs as the energy donor. It's well known that there is no photobleaching when BQDs is irradiated by the excitation light, which makes the FRET system very stable. Secondly, using ratio fluorescence analysis to detect the target eliminates the impacts of environmental changes and of the instability of the test instrument. Thirdly, this assay has a good selectivity. Many co-existing anions, reactive oxygen species, reducing substances and biological mercaptan in the biological samples have no interference with the detection of HSO_3^-. Considering these advantageous characteristics, we anticipate the proposed ratiometric fluorescence assay will be very useful for physiological and pathological studies of SO_2.

Conflicts of interest

There are no conflicts to declare.

Acknowledgements

Financial support from the Natural Science Foundation of China (No. 201575031 to SZ), the U.S. National Institutes of Health (GM089557 to YML) and Natural Science Foundation of Guangxi Province (No. 2017GXNSFFA198014) as well as BAGUI Scholar Programs is gratefully acknowledged.

References

1 A. V. Leontiev and D. M. Rudkevich, *J. Am. Chem. Soc.*, 2005, **127**, 14126–14127.
2 D. P. Li, Z. Y. Wang, X. J. Cao, J. Cui, X. Wang, H. Z. Cui, J. Y. Miao and B. X. Zhao, *Chem. Commun.*, 2016, **52**, 2760–2763.
3 Y. Liu, K. Li, K. X. Xie, L. L. Li, K. K. Yu, X. Wang and X. Q. Yu, *Chem. Commun.*, 2016, **52**, 3430–3433.
4 T. Finkel and N. J. Holbrook, *Nature*, 2000, **408**, 239–247.
5 M. H. Stipanuk and I. Ueki, *J. Inherited Metab. Dis.*, 2011, **34**, 17–32.
6 Z. Meng, Z. Yang, J. Li and Q. Zhang, *Chemosphere*, 2012, **89**, 579–584.
7 G. Li and N. Sang, *Ecotoxicol. Environ. Saf.*, 2009, **72**, 236–241.
8 N. Sang, Y. Yun, H. Li, L. Hou, M. Han and G. Li, *Toxicol. Sci.*, 2010, **114**, 226–236.
9 D. R. Shankaran, N. Uehera and T. Kato, *Sens. Actuators, B*, 2002, **87**, 442–447.
10 R. F. McFeeters and A. O. Barish, *J. Agric. Food Chem.*, 2003, **51**, 1513–1517.
11 G. Jankovskiene, Z. Daunoravicius and A. Padarauskas, *J. Chromatogr. A*, 2001, **934**, 67–73.
12 Y. Sun, P. Wang, J. Liu, J. Zhang and W. Guo, *Analyst*, 2012, **137**, 3430–3433.
13 H. Xie, F. Zeng, C. Yu and S. Wu, *Polym. Chem.*, 2013, **4**, 5416–5424.
14 X. Yang, M. Zhao and G. Wang, *Sens. Actuators, B*, 2011, **152**, 8–13.
15 Y. Yang, F. Huo, J. Zhang, Z. Xie, J. Chao, C. Yin, D. Liu, S. Jin and F. Cheng, *Sens. Actuators, B*, 2012, **166**, 665–670.
16 C. Yu, M. Luo, F. Zeng and S. Wu, *Anal. Methods*, 2012, **4**, 2638–2640.
17 M. Choi, J. Hwang, S. Eor and S. Chang, *Org. Lett.*, 2010, **12**, 5624–5627.
18 X. Gu, C. Liu, Y. Zhu and Y. J. Zhu, *J. Agric. Food Chem.*, 2011, **59**, 11935–11939.
19 X. H. Cheng, H. Z. Jia, J. Feng, J. G. Qin and Z. Li, *Sens. Actuators, B*, 2013, **184**, 274–280.
20 W. Chen, Q. Fang, D. Yang, H. Zhang, X. Song and J. Foley, *Anal. Chem.*, 2015, **87**, 609–616.
21 S. Chen, P. Hou, J. Wang and X. Song, *RSC Adv.*, 2012, **2**, 10869–10873.
22 M. Y. Wu, K. Li, C. Y. Li, J. T. Hou and X. Q. Yu, *Chem. Commun.*, 2014, **50**, 183–185.
23 L. M. Zhu, J. C. Xu, Z. Sun, B. Q. Fu, C. Q. Qin, L. T. Zeng and X. C. Hu, *Chem. Commun.*, 2015, **51**, 1154–1156.
24 H. Yu, L. B. Du, L. M. Guan, K. Zhang, Y. Y. Li, H. J. Zhu, M. T. Sun and S. H. Wang, *Sens. Actuators, B*, 2017, **247**, 823–829.
25 J. B. Chao, X. L. Wang, Y. M. Liu, Y. B. Zhang, F. J. Huo, C. X. Yin, M. G. Zhao, J. Y. Sun and M. Xu, *Sens. Actuators, B*, 2018, **272**, 195–202.
26 Y. Q. Zhang, D. K. Ma, Y. Zhuang, X. Zhang, W. Chen, L. L. Hong, Q. X. Yan, K. Yu and S. M. Huang, *J. Mater. Chem.*, 2012, **22**, 16714–16718.
27 D. P. Li, Z. Y. Wang, X. J. Cao, J. Cui, X. Wang, H. Z. Cui, J. Y. Miao and B. X. Zhao, *Chem. Commun.*, 2016, **52**, 2760–2763.
28 Y. Liu, K. Li, K. X. Xie, L. L. Li, K. K. Yu, X. Wang and X. Q. Yu, *Chem. Commun.*, 2016, **52**, 3430–3433.
29 Y. Zhang, L. Guan, H. Yu, Y. Yan, L. Du, Y. Liu, M. Sun, D. Huang and S. Wang, *Anal. Chem.*, 2016, **88**, 4426–4431.
30 M. F. Huang, L. N. Chen, J. Y. Ning, W. L. Wu, X. D. Hec, J. Y. Miao and B. X. Zhao, *Sens. Actuators, B*, 2018, **261**, 196–202.
31 J. Zhu, F. Qin, D. Zhang, J. Tang, W. Liu, W. Cao and Y. Ye, *New J. Chem.*, 2019, **43**, 16806–16811.
32 S. Sahu, B. Behera, T. K. Maiti and S. Mohapatra, *Chem. Commun.*, 2012, **48**, 8835–8837.
33 J. Wang, C. F. Wang and S. Chen, *Angew. Chem., Int. Ed.*, 2012, **51**, 1–6.
34 J. Zhao, M. Huang, L. Zhang, M. Zou, D. Chen, H. Huang and S. Zhao, *Anal. Chem.*, 2017, **89**, 8044–8049.

35 A. Mewada, S. Pandey, S. Shinde, N. Mishra, G. Oza, M. Thakur, M. Sharon and M. Sharon, *Mater. Sci. Eng., C*, 2013, **33**, 2914–2917.
36 W. J. Lu, X. J. Gong, M. Nan, Y. Liu, S. M. Shuang and C. Dong, *Anal. Chim. Acta*, 2015, **898**, 116–127.
37 Y. Q. Dong, H. C. Pang, H. B. Yang, C. X. Guo, J. W. Shao, Y. W. Chi, C. M. Li and T. Yu, *Angew. Chem.*, 2013, **125**, 7954–7958.
38 A. Prasannan and T. Imae, *Ind. Eng. Chem. Res.*, 2013, **52**, 15673–15678.
39 P. C. Hsu, Z. Y. Shih, C. H. Lee and H. T. Chang, *Green Chem.*, 2012, **14**, 917–920.
40 J. Zhou, Z. Sheng, H. Han, M. Zou and C. Li, *Mater. Lett.*, 2012, **66**, 222–224.
41 W. Lu, X. Qin, A. M. Asiri, A. Q. Al-Youbi and X. J. Sun, *Nanopart. Res.*, 2013, **15**, 1344–1350.